Isopotential Titration for Quantifying Metal-Adsorbate Charge Transfer

Justin A. Hopkins[1,2], Shengguang Wang[1,3], Kyung-Ryul Oh[1,2], Benjamin J. Page[1,3], Jesse R. Canavan[1,2], Nondumiso Chibambo[1,2], Amber L. Walton[1,2], Sallye R. Gathmann[1,2], Jason A. Chalmers[1,4], Susannah L. Scott[1,4], Matthew Neurock[1,2], Lars C. Grabow[1,3], James R. McKone[5], Paul J. Dauenhauer[1,2,*], Omar A. Abdelrahman[1,3,*]

[1] Center for Programmable Energy Catalysis, University of Minnesota, Department of Chemical Engineering & Materials Science, 421 Washington Ave. SE, Minneapolis, MN, USA, 55455, cpec.umn.edu
[2] Department of Chemical Engineering & Materials Science, University of Minnesota, 421 Washington Ave. SE, Minneapolis, MN, USA, 55455
[3] William A. Brookshire Department of Chemical and Biomolecular Engineering, University of Houston, 4226 Martin Luther King Blvd., Houston, TX, USA 77204
[4] Department of Chemical Engineering, University of California-Santa Barbara, Engineering II, Santa Barbara, CA, 93106
[5] Department of Chemical and Petroleum Engineering, University of Pittsburgh, 3700 O'Hara St, Pittsburgh, PA, USA, 15213
* Corresponding authors: oabdel@uh.edu, hauer@umn.edu

Abstract. The extent of charge transfer between adsorbed reactants and a catalyst surface plays a key role in determining binding energy and catalytic activity. Here, we describe the technique of 'isopotential titration' (IPT) to quantify the magnitude and direction of charge transfer between adsorbates and catalytic surfaces. The method used a 'catalytic condenser' device (Pt/C/70 nm HfO_2/p^{++}-Si) to evaluate the adsorption of hydrogen on a platinum-on-carbon conductive surface on a HfO_2 (70 nm) film on a silicon wafer, with a potentiostat applying fixed (zero) voltage between the conductive Pt/C and silicon wafer layers. Dissociative adsorption of hydrogen on Pt resulted in electron flow through the external circuit from the Pt electrode toward the Si substrate, indicating that adsorbed hydrogen atoms donated electron density to the Pt surface, which then equilibrated with electrons flowing through the potentiostat to the silicon substrate. Desorption of hydrogen from the Pt surface exhibited equal and opposite current flow. The magnitude of the measured charge transfer upon hydrogen adsorption increased with increasing temperature from 100 to 200 °C, consistent with a larger change in H surface coverage at higher temperatures for cycling gaseous H_2 partial pressures between 0.5% and 99.999%. Charge transferred from H atoms to the Pt was estimated as 0.17% of an electron donated per adsorbed H atom. The extent of charge transfer was comparable with a computed Bader charge analysis, which calculated an average of 0.4% of an electron transferred from adsorbing H to Pt at high surface coverage. With hydrogen adsorption being an example, isopotential titrations provide a new tool to quantify charge transfer events in heterogeneous catalytic systems.

Introduction. Heterogeneous catalysis is enabled by a surface's ability to lower activation energies of chemical reactions through temporary bonding. Along a reaction coordinate, electrons are transferred during bond breaking and forming events between adsorbates and the catalytic surface. The enthalpy released upon formation of surface-adsorbate bonds permits otherwise stable bulk-phase molecules to lose entropy while chemisorbing on catalyst surfaces and begin catalytic reaction cycles.[1] The energy of such surface-adsorbate bonds relative to their initial unbound states (i.e., binding energy) is therefore an effective descriptor for catalytic activity, with a catalytic rate optimum existing for a reaction per the Sabatier principle.[2–6] Therefore, it is not surprising that a catalyst's inherent ability to transfer electrons to or from the reactants (via Lewis acidity and the *d*-band center for solid acid[7–11] and metal catalysts,[12–14] respectively) strongly correlates with catalytic reaction rates.

Charge transfer is not unique to heterogeneous catalysis, as it is critical to the other catalytic fields. For homogeneous catalysis, the oxidation states of metal centers often change throughout reaction cycles to accommodate changes in metal center coordination (e.g. Wilkinson's catalyst[15,16]), and electrocatalysis applies surface potentials to drive the electron transfer processes.[17,18] Charge transfer in electrochemistry enables ordinarily nonspontaneous reactions to be driven to appreciable rates.[17–19] The ability to use charge-

voltage work to modulate reaction free energies is shown in **Equation 1** where $\frac{\partial G}{\partial \chi}$ is the differential of the Gibbs free energy with respect to the reaction coordinate (in moles),

$$\frac{\partial G_i}{\partial \chi} = dG_i^o + \delta F \phi \quad (1)$$

dG_i^o is the molar free energy change under a suitable reference condition (e.g., zero applied voltage), δ is the extent of charge transfer through the reaction coordinate, F is Faraday's constant, and ϕ is the potential difference between catalyst surface and surface intermediates. The product of the electrons transferred, Faraday's constant, and the potential difference represents the work (in energy per mole) driven into/out of the system over the reaction coordinate,

$$W = \delta F \phi \quad (2)$$

This charge-voltage work can drive the free energy change over this reaction coordinate negative (i.e., $\frac{\partial G}{\partial \chi} < 0$) making an otherwise nonspontaneous reaction ($dG_{rxn}^o > 0$) occur.

Many phenomena result in electric potential gradients across catalyst surfaces including supporting catalysts on materials with different Fermi levels[20–25] and addition of catalyst promoters.[26–28] **Equation 1** implies that the intentional creation of a potential gradient influences both the free energy change along a reaction coordinate and the associated catalytic activity. Changes in catalytic rates and/or selectivity as a result of an applied electric field, whether directly to catalyst beds, via electrodes, or by surface plasmons, have been reported.[29–35] However, research to date has not uncoupled the extent of charge transfer from applied voltages, focusing instead on overall catalytic effects with applied voltages or electric fields. More research is needed to understand: (1) how catalyst synthesis choices influence potential gradients across interfaces, and (2) quantification of charge transfer events along reaction coordinates. Understanding the magnitude and direction of partial charge transfer within elementary steps on a catalytic surface will help identify reactions susceptible to charge-voltage work effects.

Electron transfer between catalyst surfaces and adsorbates in the liquid phase has been documented through measurements of catalyst electronic properties.[36–38] However, evidence of charge transfer between catalyst surfaces and molecules adsorbing from the gas phase is limited, with most studies performed under ultrahigh vacuum conditions. The most direct evidence of electron transfer between adsorbates and catalyst surfaces is shown through the complementary ultraviolet photoelectron spectroscopy (UPS)[39–43] and Kelvin probe measurements.[44–46] With these techniques, researchers have shown that adsorbates change the work functions of metals, suggesting that adsorbates change the occupancy of electronic states near the Fermi level at the metal surface (i.e., charge transfer). For example, Christmann, Ertl, and Pignet showed that the adsorption of H_2 on Pt(111) at high coverages lowered the work function of Pt.[39] Kiskinova, Pirug, and Bonzel showed that water as an adsorbate lowered the work function of Pt(111), but increased it on K-covered surfaces.[40] However, none have been able to directly quantify the amount of charge transfer between adsorbate and catalyst surface, only indicating a change in the potentials of the surface.

Recently, we reported on 'catalytic condensers,' in which a nanometer-scale catalyst layer is placed atop a thin film parallel plate capacitor.[47–50] We showed that applying potential across the condenser dielectric film altered the electronic properties of the catalyst top layer, modulating the activation energy of isopropanol dehydration on Al_2O_3[47] and the binding energy of CO* on Pt[48–50]. Changes in surface binding energies were linear with respect to voltage, consistent with the expected linear change in free energy along a reaction coordinate as a result of charge transfer events (**Equation 1**). While the design of the catalytic condenser enables the variation of surface energetics through applied voltages, it also quantifies the extent of charge transfer between adsorbates and the underlying catalyst surface.

In this work, we experimentally and computationally quantified charge transfer events between hydrogen adsorbates and Pt surfaces by via the new method of 'isopotential titration' (IPT) on catalytic condensers. As depicted in **Figure 1A**, a generic adsorption event on a catalyst site (*) yields fractional charge transfer, δ e^-.[36] For example, dissociative adsorption of H_2 to top or fcc sites on Pt(111) is known to result in surface-adsorbate dipoles consistent with charge transfer, as shown in

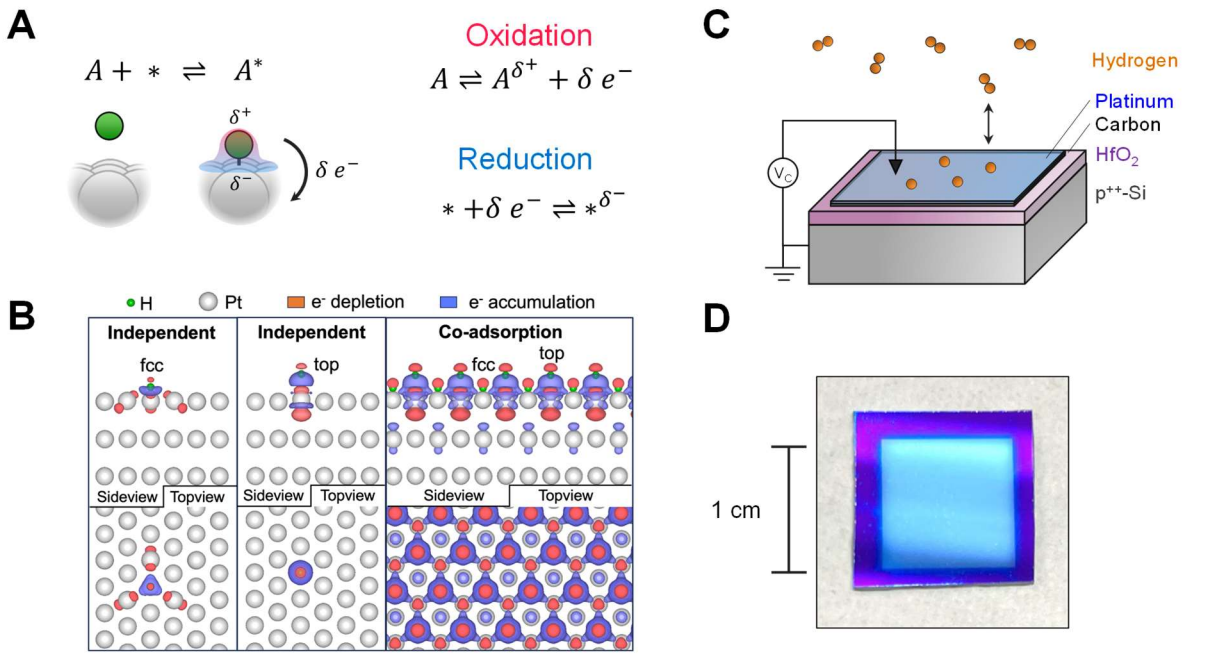

Figure 1. **(A)** A generic adsorption event which involves charge transfer between the catalyst site and adsorbate and can thus be split into an oxidation and reduction half-cell reaction. **(B)** Charge density difference analysis of H adsorption on Pt(111) surfaces when H is independently adsorbed on fcc three-fold hollow or top sites (left), and co-adsorbed in fcc and top positions at high coverage (right). **(C)** A schematic of the catalytic condensers used in this work showing the p^{++}-Si (gray), HfO_2 insulator (purple), carbon conducting layer (black), and Pt catalyst (blue). **(d)** A picture showing a Pt/C/HfO_2/p^{++}-Si device of 1 cm^2 in size.

the calculated regions of electron accumulation and depletion of H* on Pt in **Figure 1B**. When adsorption of a molecule such as H_2 occurs on the surface of a catalytic condenser (**Figure 1C**) with a fixed applied potential, the accumulated charge from adsorption flows from the top surface (e.g., Pt/C) and is measured as current flow as the device achieves electrochemical equilibrium. The extent of current flow required to achieve electrochemical equilibrium is a function of the adsorbate and surface site interaction as well as the applied fix potential, providing the capability for titrating the adsorption phenomenon (i.e., isopotential titration). Moreover, the reverse process of desorption requires equal and opposite current to restore electrochemical equilibrium of a surface of open active sites.

The amount of charge transfer across a Pt/C/HfO_2/p^{++}-Si catalytic condenser (**Figure 1D**) was experimentally quantified while varying the gas phase environment in a temperature- and pressure-controlled chamber. The results indicated that a change in the chemical environment induces a current from the Pt surface that is reproducible upon sequential adsorption and desorption of H_2, and the trends in temperature and gas composition correlate with changes in the equilibrium surface coverage of H*. The titrated charge for conditions of predictable surface coverage of H* was compared with calculated charge transfer showing agreement between experimental measurements and calculations.

Results and Discussion. In isopotential titration (IPT) experiments, a 1 cm^2 of 1 nm Pt/3 nm C/62 nm HfO_2/p^{++}-Si condenser device was fabricated by existing methods and electronically evaluated prior to use.[48,49] The working electrodes of the potentiostat were attached to the Pt electrode, while the counter and reference electrodes were attached to the p^{++}-Si. Positive measured current means electrons were flowing from the Pt surface through the potentiostat to the Si support. Each device was tested using cyclic voltammetry (CV) to confirm

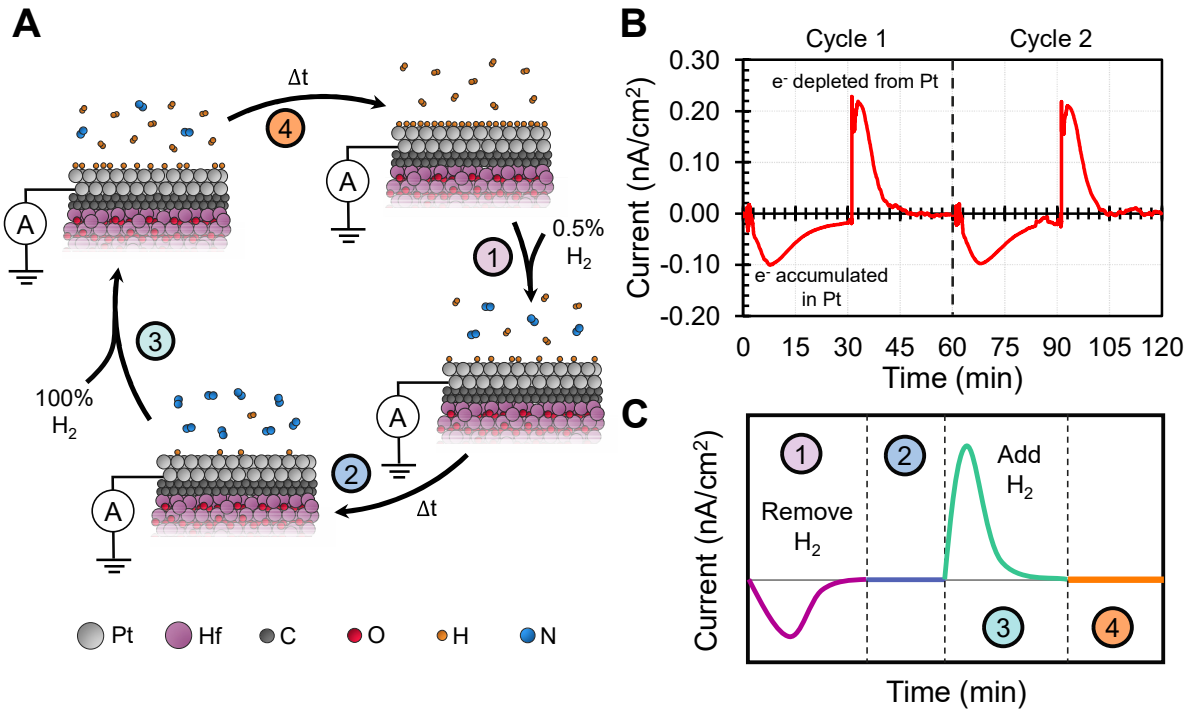

Figure 2. **The Isopotential Titration (IPT) Method. (A)** A schematic of the Pt condenser surface cycling between high and low H* coverage under flow of 99.999% H_2 and 0.5% H_2, respectively, during isopotential titration experiments. **(B)** The current versus time graph of an isopotential titration experiment at 250 °C with markers linking the time on the graph to the cycle in panel a schematic. **(C)** A cartoon of the isopotential titration experiment splitting the time-series data into the steps shown in panel **1A**.

the integrity of the device electronic properties at room temperature prior to use (i.e., capacitance near 200 nF/cm^2 and leakage resistances near 100 MΩ). Cyclic voltammograms for each device used in this study are included in the supporting information. Additionally, each device was heated to 250 °C and then reduced in 50 sccm of flowing H_2 for 30 minutes. Device initialization comprised setting the potentiostat to 0 V overnight to allow each device to achieve electrochemical equilibrium prior to the start of adsorption/desorption experiments. Establishing this initial equilibrium was critical to an accurate measurement of adsorption current, because further electronic equilibration currents would convolute the isopotential titration experiments. Prior to each isopotential titration trial, the reactor temperature was set using a PID heating loop and the device's electronic integrity was confirmed via CV.

Isopotential titration experiments were started by applying 0 V and flowing 50 sccm of 99.999% H_2 for 30 minutes to ensure that the initial state of the catalyst was mostly H* covered Pt in electronic equilibrium with p^{++}-Si. Every 30-minutes thereafter, the gas flow was switched between 0.5% H_2 in N_2 (we do not expect the N_2 to chemisorb to the surface at the experimental conditions tested) and 99.999% H_2 using a gas switching valve. Additionally, a bellows pump was used between some experiments to generate a weak vacuum to remove H_2 from the chamber to rapidly reset the system. The experimental cycle for these isopotential titration experiments is depicted in **Figure 2A**. The surface was cycled multiple times at each temperature before switching to a new temperature setpoint.

Figure 2B shows the current over time during an experiment at 200 °C. Upon switching the inlet gas to 0.5% H_2 at the zero-minute mark, there was a broad negative current peak that returned to the baseline within 15 minutes. This time scale is consistent with the hydraulic time scale of the reactor for achieving a steady state composition. In contrast, the switch to pure H_2 flow (starting at 30

minutes) induced a sharper, positive current peak with the current returning to the baseline of about zero amps (0 A) in less than 15 minutes. The H_2 adsorption peak was likely sharper due to the more favorable kinetics of dissociative H_2 adsorption, relative to that of the associative desorption of H* from the Pt surface.[51] The two peaks were consistent over multiple cycles demonstrating that this process was repeatable for the same device at the same conditions. There is a clear and repeatable current peak every time the composition of the reactor changes, indicating that this effect is related to the change in chemical environment. Furthermore, the measured currents did not depend on the capacitance of the catalytic condenser. As long as the device remained insulating in nature (i.e., the resistance of the wires and Pt/C is much less than that of the HfO_2) the currents were measured to consistent values (see **Section 4C** of the Supporting Information).

Additionally, we considered the possibility that the measured current was due to energy transfer between the adsorbing H_2 and the Pt. Previous studies of catalytic nanodiodes (i.e., devices without the insulating layer) exhibited current flow over a Schottky barrier, which was ascribed to non-adiabatic heat transfer which converted the energy released by the exothermic adsorption to electron-hole pair formation in the metal catalyst.[52–54] This is likely a different phenomenon than observed in our catalytic condensers, because we see current for both exothermic adsorption of H_2 (i.e., switching to higher H_2 concentration) and for endothermic desorption (i.e., switching to lower concentrations).

Regarding the change in thermal conductivity of the gases when switched between pure H_2 and 0.5% H_2 in N_2, the current produced by these changes in the device via slight variation in heating from an external heat jacket were small (1-100 pA) and opposite in sign when compared to the current peaks (1-10 nA) measured for H_2 adsorption and desorption. These results are presented in **Sections 4B** and **4C** of the Supporting Information.

Confirming that current peaks are repeatable and unconvoluted by device, energetic, and thermal artifacts suggests that the current observed is a specific electrical interaction between the Pt and the adsorbing H_2. This conclusion is not controversial for single crystal ultrahigh vacuum studies. As mentioned before, researchers used techniques such as Kelvin probe or ultraviolet photoelectron spectroscopy to measure the change in Pt(111) work function between clean surface and the surface covered with H*.[39,41] The authors found definitive evidence that adsorbed hydrogen changes the work function, and therefore the Fermi level of electrons, in Pt. In our experiments, a change in the Fermi level of Pt would result in Pt being out of electronic equilibrium with the p^{++}-Si. Therefore, to re-establish equilibrium, current must flow between the Pt and p^{++}-Si. Specifically, adsorbing H_2 yields positive current peaks meaning that electrons are transported from the Pt to the p^{++}-Si. This suggests that H_2 is decreasing the work function of Pt/C system (i.e., increasing the chemical potential of an electron in the Pt) such that electrons flow from the Pt/C to p^{++}-Si. This trend of H_2 adsorption decreasing the work function of Pt is consistent with the moderate-to-high H* coverage results on Pt(111) from Christmann, Ertl, and Pignet and on Pt 6(111)x(100) from Collins and Spicer.[39,41]

If the measured current is due to re-equilibration, then this process should be cyclic and reversible if the reactor-device system is given sufficient time to equilibrate. Therefore, the net charge transferred over one full surface cycle (i.e., desorb H* in 0.5% H_2 flow, adsorb H* in 100% H_2) should be zero. Furthermore, each time the surface is cycled, the charge should be consistent. This is shown in **Figure 3A** where the magnitude of the charge transferred (i.e., the current peaks integrated over time) for both the adsorption (positive current) and desorption (negative current) peaks are normalized to the first adsorption peak area and plotted for three temperatures (100, 150, and 200 °C). These data indicate that the transferred charge upon H_2 adsorption and desorption is repeatable and cyclic within experimental error, as expected from an equilibrating process.

The data also show that the measured current is a function of temperature (**Figure 3B**), which also indicates that the current is associated with adsorption of H_2. Despite switching between nearly 100% H_2 and 0.5% H_2 in the experimental chamber, the surface coverage of H* does not change between 100% and 0%, since fully covered or fully empty surfaces are energetically prohibitive, especially at atmospheric pressures. According to literature data from Hibbitts and Iglesia on H_2 adsorption to Pt/Al_2O_3, the H* coverage at 0.5% H_2 is still over 95% at 100 °C.[55] **Figure 3C** shows the Langmuir isobar calculated from these data. Taking

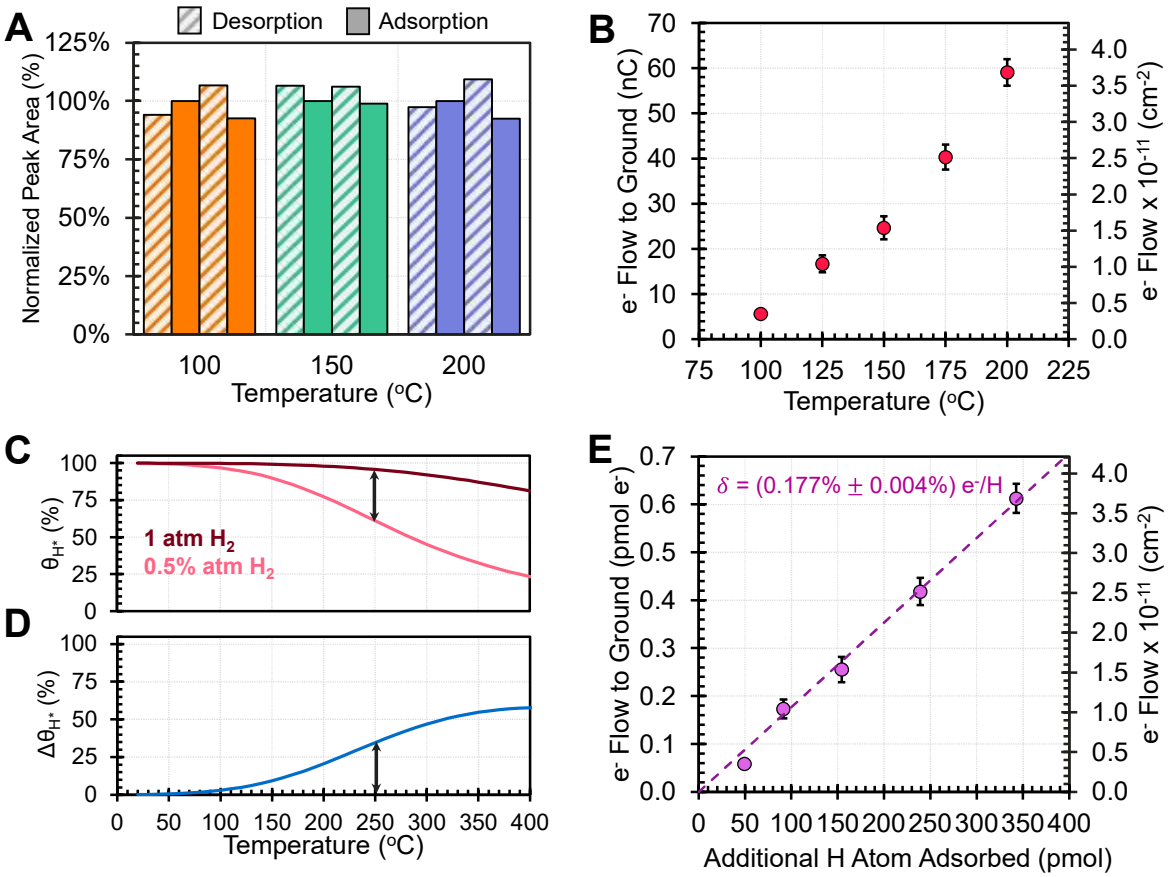

Figure 3. **(A)** The peak area for H_2 adsorption and desorption at 100, 150, and 200 °C with the values normalized to the first adsorption peak area to demonstrate the cyclic nature of these experiments. **(B)** The integral of the current over time versus the temperature (with 95% confidence intervals) for each isopotential titration experiment. **(C)** The calculated surface coverage of H_2 on Pt versus temperature for 1 atm H_2 partial pressures and for 0.005 atm H_2 partial pressures from literature data. **(D)** The difference in H* coverage between the 1 atm isobar and 0.005 atm isobar at each temperature shown in subpanel **3c** which represents the expected change in coverage at each temperature in the isopotential titration experiments, **(E)** A graph of the magnitude of charge transferred (with 95% confidence intervals) versus the calculated amount of H atoms adsorbed demonstrating a linear trend.

the difference between the coverage of the two isobars at a given temperature in **Figure 3D** predicts the expected change in Pt surface coverage over the course of these experiments (99.999% H_2 versus 0.5% H_2) at any given temperature. Overall lower changes of surface coverage during adsorption cycling is predicted when operating at lower temperatures, which is consistent with our results of smaller amount of charge transferred upon adsorption and desorption of H_2 at lower temperatures.

The interpretation of the quantity of charge transferred when switching the surface coverage of hydrogen remains in question. In fabricating catalytic condensers, nanometer-scale catalyst layers are imperative to observing voltage effects during temperature programmed desorption experiments.[48] A direct consequence of this is that the total number of charge carriers in the Pt (which has a high *density* of carriers) is far outnumbered by that of the p^{++}-Si which has a charge carrier density that is ~1000 times less than Pt[56,57] but is also 10^6 times thicker. In fact, the maximum number of electrons transferred in these experiments would only change the charge carrier density of the p^{++}-Si by 1 ppm. Following the calculations in **Section 6** in the Supporting Information, the direct result is that the p^{++}-Si acts as a charge carrier sink, which has been observed in other catalytic systems where the metal catalyst is scarce as compared to a

semiconductor.[21,25] In other words, any excess charge carriers transferred to the Pt will flow into the p^{++}-Si to establish an equilibrium.

The equilibrium driving force for electrons to flow from Pt to the Si upon hydrogen adsorption also requires a pathway for current flow. The resistance for current to pass through the potentiostat is significantly lower than through the resistive HfO_2 condenser layer, so any excess charge carriers added to the Pt will pass through the potentiostat. Charge transferred during the isopotential titration experiments are therefore a direct, quantitative measure of the number of electrons exchanged between H and Pt during the formation of the surface chemisorption bond.

To quantify the adsorption-charge relationship, we assumed that the 1 cm^2 of Pt contains about 10^{15} sites/cm^2. Site density allows for determination of the H* coverage to be compared with the measured total current to obtain an estimate of the extent of charge transfer, δ, in **Equation 1**. Plotting the molar quantity of electrons transferred versus this quantity, as shown in **Figure 3E**, indicates a linear relationship between the current observed and the calculated amount of H_2 adsorbed. From this relationship, we can extract the value of $(+0.177 \pm 0.004)\%$ of a elementary charge per H atom adsorbed to the Pt over the range of hydrogen coverages considered in this experiment. We further considered other literature adsorption thermodynamics for H_2 on Pt to evaluate the range of possible hydrogen surface coverages and resulting charge transfer values measured in these experiments with the analysis shown in **Section 5C** in the Supporting Information. Following these calculations, we find that the value of δ calculated from our experiments is bracketed between +0.1% and +0.4% based on ranges of experimental adsorption thermodynamics that were found in literature.[58–60]

Hydrogen atoms have a weak site preference and can adsorb to both fcc three-fold hollow sites and atop sites on Pt(111) surfaces with different polarity at low coverage as shown in **Figure 4A**.[41,61]. To quantify charge transfer at the higher coverages encountered in the IPT experiments, we used a Bader charge analysis[62] to calculate an average charge per H* adsorbate for varying surface coverages of 1.6, 14.7, and 29.3 H/nm^2, shown in **Figure 4B.** The Bader charges were extracted from density functional theory calculations (DFT) using the Perdew–Burke–Ernzerhof (PBE)[63] generalized gradient approximation (GGA)[64] functional and a four-layer Pt(111)-(3×3) slab model with periodic boundary conditions.

At low coverages (1.6 H/nm^2, equivalent to one H* per nine surface Pt atom) the H atoms on fcc sites are charged to -2.0% of an elementary charge, while H* on atop sites carry an opposite charge of +1.3%. Assuming an equal population of atop and fcc sites we can estimate an average charge of -0.35% of an elementary charge per H* (with respect to a neutral surface). At moderate coverages of 14.7 H/nm^2, equivalent to one H* per surface Pt atom, H atoms on fcc sites become slightly less negatively charged at -1.8% e/H. Interestingly, atop sites begin to flip in polarity in this moderate coverage regime and retain almost no charge. Overall, the average charge per H* adsorbate at 14.7 H/nm^2 is -0.95% e/H if both atop and fcc sites are occupied equally. When all atop and fcc sites are covered simultaneously at 29.3 H/nm^2, the polarities of H* on fcc and atop sites become large in magnitude and opposite in value compared to the low coverage case. In this regime, H* on fcc sites has flipped from negative polarity to +5.2% e/H, while atop H* becomes negative resulting in a charge of -4.4% e/H. The overall average charge per H* was +0.40% e/H. Overall, these results show that the net charge transferred upon adsorption can vary significantly by which sites are being titrated and how those adsorbates influence their neighbors in different coverage regimes.

For the considered experimental conditions (100% versus 0.5% H_2, **Figure 3C**), the Pt surface always remained in the moderate to high coverage regime, suggesting that the H* adsorbed to the fcc sites could be either negatively or positively charged depending on the coverages, while atop sites should be negatively charged. Following the middle panel (14.7 H/nm^2) of **Figure 4B** to the rightmost panel (29.3 H/nm^2), we would expect the average H adsorbate to transition from negatively charged to positively charged as atoms are added from the moderate to high coverage regimes. This positive shift in charge is consistent with the results outlined in **Figure 2B** and **Figure 3B**, which showed H_2 adsorption yielding excess electrons in the Pt layer resulting in positive currents. In fact, the average charge per H* from these theoretical calculations is consistent within the same order of

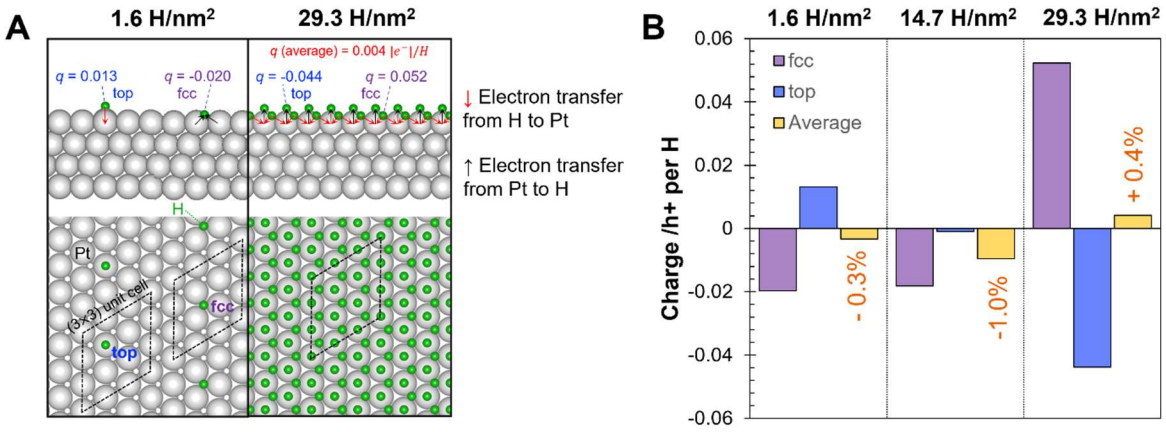

Figure 4. Bader charge analysis of electron transfer between H* and Pt(111). (A) At low coverage, H* on atop donates electron density, while H* on fcc sites withdraws electrons from Pt. At high coverage the charge transfer directions are reversed, with a net charge transfer of 0.40% $|e^-|$/H. **(B)** Coverage dependence of Bader charges on H* in atop and fcc positions at low coverage (1.6 H/nm^2), moderate coverage (14.7 H/nm^2), and high coverage (29.3 H/nm^2).

magnitude of the experimental estimate. It is worth noting that the changes in H* polarity sweeping from low coverage to high coverage has interesting consequences for catalysis where H* coverages could vary significantly based on the reaction mechanisms at play and the selected conditions. An interesting extension of these isopotential titration experiments would be to extend this technique to vacuum conditions where H* coverages could be further decreased into the low coverage regime and the computational hypothesis of changing H* polarity could be tested by dosing known amounts of H_2 into those systems.

Through both experimental and computational results, the extent of charge transfer has been estimated between H* and Pt. These results suggest that the electrochemical equilibrium of the device changes throughout the IPT experiments. **Figure 5A** schematically shows a band diagram and condenser device in N_2 gas demonstrating the initial electrochemical equilibrium between Pt, HfO_2, and the p^{++}-Si in which the Fermi levels are aligned. As H_2 is dosed into the system and H* adsorbs, the device is displaced from electrochemical equilibrium, since H* has energy states closer to the vacuum level. This results in a decrease in the work function of Pt (i.e., its Fermi level moves closer to the vacuum level) as shown in **Figure 5B**. Therefore, electrons must flow from the Pt to the p^{++}-Si (as we measure in our IPT experiments) to establish a new electrochemical equilibrium between H*, Pt, HfO_2, and p^{++}-Si shown schematically in **Figure 5B**. Once this new electrochemical equilibrium is achieved, no additional electrons flow as shown in **Figure 5C**. With this diagram in mind, IPT experiments provide an experimental method to quantify the differences in the occupancy of adsorbate electronic states near the Fermi level of the metal catalyst. The isopotential titration (IPT) method appears general to a large number of different catalyst surfaces and adsorbates.

Conclusions. Charge transfer between adsorbates and surfaces has a critical role in heterogeneous catalysis. To this end, we developed a technique to quantify charge transfer between surface species and catalyst surfaces referred to as 'isopotential titration.' In these experiments, the Pt surface of a catalytic condenser was cycled between atmospheres of high and low concentrations of H_2 to change the coverage of H* on the surface. Current between the Pt surface and a silicon charge carrier reservoir was measured using a potentiostat at zero applied voltage. The current integrated over time (i.e., total charge) after introducing 99.999% H_2 to the Pt condenser yielded repeatable positive peaks in current, while the integrated current over time while depleting the vessel with the Pt condenser of H_2 were negative and equal in

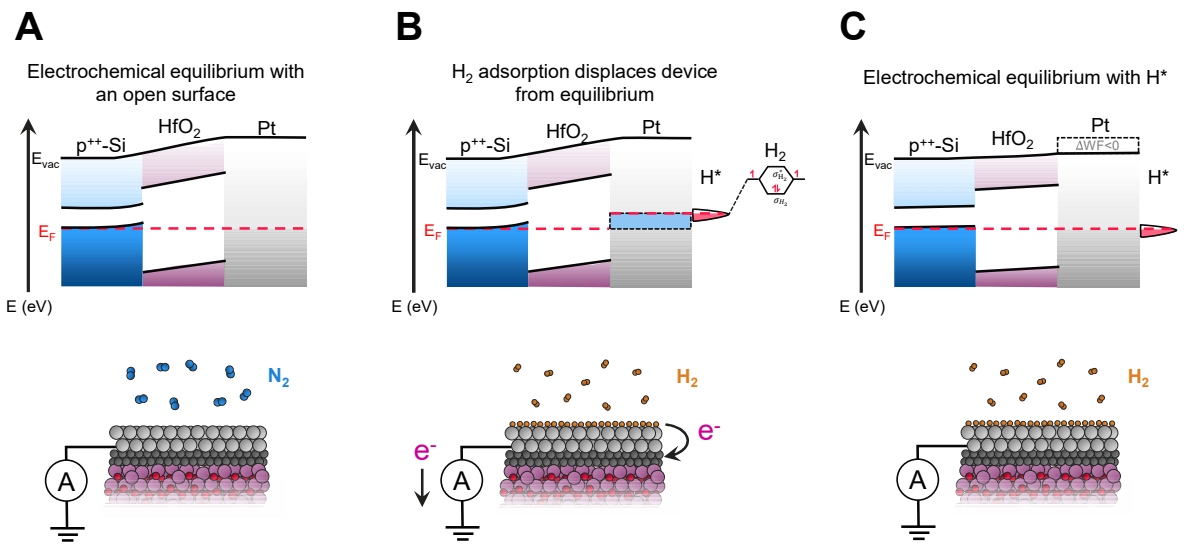

Figure 5. (A) A qualitative band diagram of the catalytic condenser in N_2 gas showing the p^{++}-Si, HfO_2, and Pt layers with equilibrated Fermi levels and a Pt surface with open sites. **(B)** A band diagram showing H_2 dissociative adsorption displacing the original electrochemical equilibrium along with a schematic of a device adsorbing H_2 and transferring electrons from the H* to the Pt and then to the grounded Si. **(C)** A band diagram showing the p^{++}-Si, HfO_2, Pt, and H* in electrochemical equilibrium where no additional electron flow occurs with a device at steady state H* coverage.

magnitude to the adsorption peaks. These positive currents for hydrogen adsorption are consistent with experimental results in ultrahigh vacuum studies and indicate that H atoms donate electrons to Pt upon adsorbing in the coverage regimes encountered in these experiments.

Furthermore, larger currents were measured upon adsorption and desorption of H_2 as the temperature increased, which was shown to be consistent with larger changes in hydrogen surface coverage determined from literature-reported isotherms at each temperature. Using these surface coverage models, we calculated that approximately $(0.177 \pm 0.002)\%$ of an electron was transferred to the Pt surface per H atom adsorbed. The direction and relative magnitude of charge transfer measured between the Pt surface and the Si charge reservoir agreed with a Bader charge analysis at moderate to high coverage.

Overall, isopotential titrations provide a new experimental tool to identify and measure charge transfer phenomena in heterogeneous catalyst surfaces with bountiful combinations of materials and adsorbates for examination. Molecules beyond H_2, such as CO and NH_3, are important in many reactions and are strong adsorbers on metals and may exhibit greater charge transfer with the surface. Beyond adsorption, isopotential titrations can be used to analyze surfaces of mixed species, such as the complex surface state during chemical reactions. Additionally, the extent of adsorbate-to-surface charge transfer provides insight into the requirements for programmable catalytic surfaces, which aim to modulate surface charge density to dynamically control catalyst surface chemistry. With the isopotential titration technique, measurements of charge transfer could provide fundamental knowledge of charge-voltage-material effects throughout heterogeneous catalysis that will allow us to unify the subfields of catalysis.

Methods. *Catalyst device fabrication and characterization.* Catalytic condensers were fabricated with Pt as the catalyst, C as a conducting support, HfO_2 as an insulator, and p^{++}-Si as the substrate in a Class 100 cleanroom. To start, a 4", approximately 0.5 mm thick degeneratively p-doped Si wafer from Wafer Pro was used. The resistivity of the wafer according to the supplier was less than 0.005 Ω cm. HfO_2 was deposited over the whole wafer using atomic layer deposition (ALD) using a Kurt J. Lesker ALD-150LE with

tetrakis(dimethylamido)hafnium (IV) (TDMAH, stored at 75 °C) as the precursor and water as the reactant. The Si wafer was held at 100 °C during deposition for 500 cycles, to achieve approximately 62 nm of HfO_2 (measured by ellipsometry). A shadow mask with 25 1 cm x 1 cm features was placed onto the wafer. Next, 3 nm of C was magnetron sputtered in 5 mTorr Ar at 250 W onto the masked wafer. An AJA ATC 2000 sputtering system was used with a pyrolytic carbon target. Then, ~ 1 nm of Pt was deposited onto the masked $C/HfO_2/p^{++}$-Si using electron beam evaporation using a CHA model SEC 600. Following the depositions, the 25 1 cm^2 $Pt/C/HfO_2/p^{++}$-Si were cut into pieces from the entire wafer. Chemical characterization of these devices with this architecture can be found in our previous work.[49]

Device fabrication was successful if devices could yield measurable capacitances (usually >100 nF/cm^2) and high leakage resistances (i.e., low leakage current) consistent with our previous results for $Pt/C/HfO_2/p^{++}$-Si. Cyclic voltammetry (CV) was used to calculate capacitance at voltage sweep rates from 0.50-1.50 V/s. The capacitance was determined from the slope of the current at 0 V versus sweep rate, and the leakage resistance was taken as the inverse slope of the I versus V at 0 V. Typical values at room temperature for the capacitance and leakage resistance were 220 nF/cm^2 and 100 MΩ, respectively. Room temperature CV curves are shown in **Section 1B** of the Supporting Information.

Isopotential titration experimental equipment. A reactor designed for catalytic testing of catalytic condensers was used for the isopotential titration experiments described in this work. A full process flow diagram for this equipment can be found in **Section 2A** in the Supporting Information along with additional information about the specific subunits. The reactor consists of four mass flow controllers (MFCs) combined into two separate gas streams. Each gas stream consisted of one MFC calibrated for N_2 flow, and one MFC calibrated for either 99.999% H_2 or 5% H_2 in N_2. Diluting the 5% H_2 in N_2 in additional N_2 flow resulted in the 0.5% H_2 stream used throughout this study. The gas streams could be switched between the reactor inlet and a vent using a four-port switching valve. The reactor vessel itself was made of a modified glass-to-metal CF flange system with volume of approximately 160 mL. The reactor temperature was monitored using a K-type thermocouple with the tip in the center of the glass tube in contact with the reactor gases. The thermocouple was attached to an Omega temperature controller, and heating tape and insulation surrounded the reactor to form a PID control loop. An Agilent 7890B gas chromatograph (GC) outfitted with a six-port switching valve and valve box, HP Plot Q column, a TCD, and PolyArc, and an FID was used for on-stream chemical composition analysis. Composition data points were taken automatically every five minutes since only H_2 was being detected. The potentiostat used during these experiments was a SquidStat Plus from Admiral Instruments.

Isopotential Titration Procedure. For each new device tested, the 1 cm^2 $Pt/C/HfO_2/p^{++}$-Si device was loaded into the reactor, the reactor was leak checked, and a CV test was performed at room temperature. Next, the devices were heated to 250 °C in flowing N_2 while performing chronoamperometry at 0 V. Another CV was taken after the temperature was reached, and then the device was reduced in 50 sccm 99.999% H_2 for 30 minutes. Following this, 0 V chronoamperometry was performed overnight to allow the entire device stack to reach true electrochemical equilibrium, defined here as the point where the current during chronoamperometry at 0 V was less than 10^{-11} A. Additional details on this preconditioning are provided in **Sections 3A** and **4A** of the Supporting Information.

Before each individual trial, the reactor temperature was allowed to equilibrate at the setpoint, and then a CV was measured to confirm that the device maintained its capacitance and low leakage current. Immediately following this, the reactor inlet was switched to 50 sccm of 99.999% H_2 to reduce any residual oxides and ensure maximal H* surface coverage on the Pt. Chronoamperometry was performed at 0 V for 30 minutes during this saturation period, and was continued through the remainder of the trial while also measuring the reactor composition with the GC. After this 30-minute period, the reactor inlet was switched to 50 sccm of 0.5% H_2 in N_2. After another 30 minutes, the reactor inlet was switched back to 50 sccm of 99.999% H_2 flow. A bellows pump attached to the outlet of the reactor vessel was used between experiments to generate a weak vacuum. This cycle was repeated at least twice for

each temperature. Throughout these trials, the reactor pressure was maintained at atmospheric pressures. Note that during each gas switch, the potentiostat was set to acquire data points at a faster frequency to ensure that any current changes could be resolved. The details for the sampling frequency are described in **Sections 3B** and **3C** in the Supporting Information.

Experimental Safety. Safety precautions were taken throughout these experiments, first through elimination and mitigation of hazards, then by engineering controls, and finally by personal protective equipment. During device fabrication, no unexpected hazards were encountered. The reactor used during these experiments was regularly leak checked between experiments, and the reactor was kept at atmospheric pressure to minimize leaks and reactor vessel damage. Temperatures were set as low as reasonably possible to resolve the relationships described in the results, and the PID loop contained two 10 A fuses to prevent overheating and short circuiting of the heating apparatus. Gas alarms were located in each room near the reactors to measure for H_2 and CO well below their OSHA PELs. The potentiostats were always grounded, and the maximum current allowed was 1 A.

Density functional theory (DFT). We performed DFT calculations using the Vienna Ab-initio Simulation Package (VASP)[65–70] in conjunction with the Atomic Simulation Environment (ASE)[71] structure and energy of H* on Pt(111) surface. The projected-augmented wave (PAW)[72] method was employed to describe electron-ion interactions and we selected the Perdew–Burke–Ernzerhof (PBE)[63] generalized gradient approximation (GGA)[64] functional for all our calculations. A kinetic energy cut-off of 400 eV was used for the plane-wave basis set to solve the Kohn-Sham equations. The Pt(111) surface was modeled as four-layer slab in a (3x3) unit cell with periodic boundary conditions and the bottom two layers fixed in their bulk. With the optimized lattice constant, the Pt site density in our model is 14.7 Pt/nm^2 or 1.47×10^{15} atoms/cm^2. The atoms in the bottom two layers were fixed to their bulk positions. The Brillouin zone was integrated using a (4×4×1) Monkhorst-Pack mesh[73]. To account for adsorbing molecules only on one side of the surface, a dipole correction was applied. Geometries were optimized with a force convergence criterion of 0.05 eV/Å. Bader charge analysis was performed to estimate the partial electronic charge of atoms.[62,74,75]

Acknowledgements. This work was supported as part of the Center for Programmable Energy Catalysis, an Energy Frontier Research Center funded by the U.S. Department of Energy, Office of Science, Basic Energy Sciences at the University of Minnesota under Award No. DE-SC0023464.

Keywords. Platinum, Hydrogen, Adsorption, Charge, Condenser, Titration

Supporting Information. Additional details about the device fabrication and testing (**Section 1**), the details of the reactor system (**Section 2**), the procedure used for IPT experiments (**Section 3**), the raw data and subsequent analysis (**Section 4**), the H_2 adsorption calculations (**Section 5**), and the equilibrium analysis between Pt and p^{++}-Si (**Section 6**) are found in the Supporting Information.

References.

(1) Fogler, H. S. Chapter 6: Catalysis and Catalytic Reactors. In *Elements of Chemical Reaction Engineering*; Prentice Hall, 1992.
(2) Sabatier, P. *La Catalyse En Chimie Organique*, 1st ed.; Beranger, CH., Ed.; Librairie Polytechnique.
(3) Ardagh, M. A.; Abdelrahman, O. A.; Dauenhauer, P. J. Principles of Dynamic Heterogeneous Catalysis: Surface Resonance and Turnover Frequency Response. *ACS Catal.* **2019**, *9* (8), 6929–6937. https://doi.org/10.1021/acscatal.9b01606.
(4) Medford, A. J.; Vojvodic, A.; Hummelshøj, J. S.; Voss, J.; Abild-Pedersen, F.; Studt, F.; Bligaard, T.; Nilsson, A.; Nørskov, J. K. From the Sabatier Principle to a Predictive Theory of Transition-Metal Heterogeneous Catalysis. *J. Catal.* **2015**, *328*, 36–42. https://doi.org/10.1016/j.jcat.2014.12.033.
(5) Zhang, Y.; Li, S.; Sun, C.; Wang, P.; Yang, Y.; Yi, D.; Wang, X.; Yao, J. Understanding and Modifying the Scaling Relations for Ammonia Synthesis on Dilute Metal Alloys: From Single-Atom Alloys to Dimer Alloys.

ACS Catal. **2022**, *12* (15), 9201–9212. https://doi.org/10.1021/acscatal.2c00745.

(6) Xu, G.; Cai, C.; Wang, T. Toward Sabatier Optimal for Ammonia Synthesis with Paramagnetic Phase of Ferromagnetic Transition Metal Catalysts. *J. Am. Chem. Soc.* **2022**. https://doi.org/10.1021/jacs.2c10603.

(7) Boffa, A. B.; Lin, C.; Bell, A. T.; Somorjai, G. A. Lewis Acidity as an Explanation for Oxide Promotion of Metals: Implications of Its Importance and Limits for Catalytic Reactions. *Catal. Lett.* **1994**, *27* (3–4), 243–249. https://doi.org/10.1007/BF00813909.

(8) He, W.; Potts, D. S.; Zhang, Z.; Liu, B.; Schuarca, R. L.; Hwang, S.-J.; Bond, J. Q.; Flaherty, D. W.; Cybulskis, V. J. Lewis Acidity and Substituent Effects Influence Aldehyde Enolization and C–C Coupling in Beta Zeolites. *J. Catal.* **2023**, *427*, 115105. https://doi.org/10.1016/j.jcat.2023.115105.

(9) Bregante, D. T.; Thornburg, N. E.; Notestein, J. M.; Flaherty, D. W. Consequences of Confinement for Alkene Epoxidation with Hydrogen Peroxide on Highly Dispersed Group 4 and 5 Metal Oxide Catalysts. *ACS Catal.* **2018**, *8* (4), 2995–3010. https://doi.org/10.1021/acscatal.7b03986.

(10) Ford, L.; Spanos, A.; Brunelli, N. A. Counting Sites in Lewis Acid Zeolite Sn-Beta: Connecting Site Quantification Experiments and Spectroscopy To Investigate the Catalytic Activity for the Alcohol Ring Opening of Epoxides. *ACS Catal.* **2023**, *13* (17), 11422–11432. https://doi.org/10.1021/acscatal.3c02618.

(11) Deshpande, N.; Parulkar, A.; Joshi, R.; Diep, B.; Kulkarni, A.; Brunelli, N. A. Epoxide Ring Opening with Alcohols Using Heterogeneous Lewis Acid Catalysts: Regioselectivity and Mechanism. *J. Catal.* **2019**, *370*, 46–54. https://doi.org/10.1016/j.jcat.2018.11.038.

(12) Hammer, B.; Norskov, J. K. Why Gold Is the Noblest of All the Metals. *Nature* **1995**, *376* (6537), 238–240. https://doi.org/10.1038/376238a0.

(13) Pettersson, L. G. M.; Nilsson, A. A Molecular Perspective on the D-Band Model: Synergy Between Experiment and Theory. *Top. Catal.* **2014**, *57* (1–4), 2–13. https://doi.org/10.1007/s11244-013-0157-4.

(14) Norskov, J. K.; Holloway, S.; Lang, N. D. Adsorbate–Surface and Adsorbate–Adsorbate Interactions and Their Role in Surface Reactions. *J. Vac. Sci. Technol. Vac. Surf. Films* **1985**, *3* (3), 1668–1672. https://doi.org/10.1116/1.573038.

(15) Nelson, D. J.; Li, R.; Brammer, C. Using Correlations to Compare Additions to Alkenes: Homogeneous Hydrogenation by Using Wilkinson's Catalyst. *J. Org. Chem.* **2005**, *70* (3), 761–767. https://doi.org/10.1021/jo048968r.

(16) Perea-Buceta, J. E.; Fernández, I.; Heikkinen, S.; Axenov, K.; King, A. W. T.; Niemi, T.; Nieger, M.; Leskelä, M.; Repo, T. Diverting Hydrogenations with Wilkinson's Catalyst towards Highly Reactive Rhodium(I) Species. *Angew. Chem. Int. Ed.* **2015**, *54* (48), 14321–14325. https://doi.org/10.1002/anie.201506216.

(17) Bard, A. J.; Faulkner, L. R. Chapter 3: Kinetics of Electrode Reactions. In *Electrochemical Methods Fundamentals and Applications*; Wiley, 2001.

(18) Boettcher, S. W.; Oener, S. Z.; Lonergan, M. C.; Surendranath, Y.; Ardo, S.; Brozek, C.; Kempler, P. A. Potentially Confusing: Potentials in Electrochemistry. *ACS Energy Lett.* **2021**, *6* (1), 261–266. https://doi.org/10.1021/acsenergylett.0c02443.

(19) Abdelrahman, O. A.; Dauenhauer, P. J. Energy Flows in Static and Programmable Catalysts. *ACS Energy Lett.* **2023**, 2292–2299. https://doi.org/10.1021/acsenergylett.3c00522.

(20) Schwab, G.-M. Catalytic Effects on the Surface of Semiconductors Supported by Metals. *Surf. Sci.* **1969**, *13*.

(21) Schwab, G.-M. Chemical Effects at the Solid/Solid Phase Boundary. *J. Colloid Interface Sci.* **1970**, *34* (3), 337–342. https://doi.org/10.1016/0021-9797(70)90192-X.

(22) Uenishi, T.; Sekine, Y. The Effect of Catalyst Composition on Electric Field-Mediated Catalytic Reactions for Exhaust Emission Control. *Emiss. Control Sci.*

Technol. **2023**. https://doi.org/10.1007/s40825-023-00230-3.

(23) Binninger, T.; Schmidt, T. J.; Kramer, D. Capacitive Electronic Metal-Support Interactions: Outer Surface Charging of Supported Catalyst Particles. *Phys. Rev. B* **2017**, *96* (16), 165405. https://doi.org/10.1103/PhysRevB.96.165405.

(24) Wang, Z.; Garg, A.; Wang, L.; He, H.; Dasgupta, A.; Zanchet, D.; Janik, M. J.; Rioux, R. M.; Román-Leshkov, Y. Enhancement of Alkyne Semi-Hydrogenation Selectivity by Electronic Modification of Platinum. *ACS Catal.* **2020**, *10* (12), 6763–6770. https://doi.org/10.1021/acscatal.9b04070.

(25) Gunasooriya, G. T. K. K.; Seebauer, E. G.; Saeys, M. Ethylene Hydrogenation over Pt/TiO2: A Charge-Sensitive Reaction. *ACS Catal.* **2017**, *7* (3), 1966–1970. https://doi.org/10.1021/acscatal.6b02906.

(26) Lang, N. D.; Holloway, S.; Nørskov, J. K. Electrostatic Adsorbate-Adsorbate Interactions: The Poisoning and Promotion of the Molecular Adsorption Reaction. *Surf. Sci.* **1985**, *150* (1), 24–38. https://doi.org/10.1016/0039-6028(85)90208-0.

(27) Rodriguez, JoséA.; Wayne Goodman, D. High-Pressure Catalytic Reactions over Single-Crystal Metal Surfaces. *Surf. Sci. Rep.* **1991**, *14* (1–2), 1–107. https://doi.org/10.1016/0167-5729(91)90002-F.

(28) Emmett, P. H. Studies on the Mechanism of Ammonia Synthesis over Iron Catalysts. *J. Chem. Educ.* **1930**, *7* (11), 2571. https://doi.org/10.1021/ed007p2571.

(29) Lim, C. W.; Hülsey, M. J.; Yan, N. Non-Faradaic Promotion of Ethylene Hydrogenation under Oscillating Potentials. *JACS Au* **2021**, *1* (5), 536–542. https://doi.org/10.1021/jacsau.1c00044.

(30) Seemala, B.; Therrien, A. J.; Lou, M.; Li, K.; Finzel, J. P.; Qi, J.; Nordlander, P.; Christopher, P. Plasmon-Mediated Catalytic O_2 Dissociation on Ag Nanostructures: Hot Electrons or Near Fields? *ACS Energy Lett.* **2019**, *4* (8), 1803–1809. https://doi.org/10.1021/acsenergylett.9b00990.

(31) Gorin, C. F.; Beh, E. S.; Kanan, M. W. An Electric Field–Induced Change in the Selectivity of a Metal Oxide–Catalyzed Epoxide Rearrangement. *J. Am. Chem. Soc.* **2012**, *134* (1), 186–189. https://doi.org/10.1021/ja210365j.

(32) Yamano, R.; Ogo, S.; Nakano, N.; Higo, T.; Sekine, Y. Non-Conventional Low-Temperature Reverse Water–Gas Shift Reaction over Highly Dispersed Ru Catalysts in an Electric Field. *EES Catal.* **2023**, *1* (2), 125–133. https://doi.org/10.1039/d2ey00004k.

(33) Zhang, R.; Zhang, J.; You, H.; Amin, M. U.; Li, J.-F.; Fang, J. Driving Reactant Molecules to Plasmonic Active Sites Using Electric Field for Enhanced Catalytic Reaction. *ACS Catal.* **2023**, 12021–12029. https://doi.org/10.1021/acscatal.3c03125.

(34) Lee, V.-J. Heterogeneous Catalysis: Effect of an Alternating Electric Field. *Science* **1966**, *152* (3721), 514.

(35) Che, F.; Gray, J. T.; Ha, S.; Kruse, N.; Scott, S. L.; McEwen, J.-S. Elucidating the Roles of Electric Fields in Catalysis: A Perspective. *ACS Catal.* **2018**, *8* (6), 5153–5174. https://doi.org/10.1021/acscatal.7b02899.

(36) Schmickler, W.; Guidelli, R. The Partial Charge Transfer. *Electrochimica Acta* **2014**, *127*, 489–505. https://doi.org/10.1016/j.electacta.2014.02.057.

(37) Wesley, T. S.; Román-Leshkov, Y.; Surendranath, Y. Spontaneous Electric Fields Play a Key Role in Thermochemical Catalysis at Metal−Liquid Interfaces. *ACS Cent. Sci.* **2021**, *7* (6), 1045–1055. https://doi.org/10.1021/acscentsci.1c00293.

(38) Schultze, J. W.; Vetter, K. J. Experimental Determination and Interpretation of the Electrosorption Valency γ. *J. Electroanal. Chem. Interfacial Electrochem.* **1973**, *44* (1), 63–81. https://doi.org/10.1016/S0022-0728(73)80515-7.

(39) Christmann, K.; Ertl, G.; Pignet, T. Adsorption of Hydrogen on a Pt(111) Surface. *Surf. Sci.* **1976**, *54* (2), 365–392.

https://doi.org/10.1016/0039-6028(76)90232-6.
(40) Kiskinova, M.; Pirug, G.; Bonzel, H. P. Adsorption and Decomposition of H2O on A K-Covered Pt(111) Surface. *Surf. Sci.* **1985**, *150*, 319–338.
(41) Collins, D. M.; Spicer, W. E. The Adsorption of CO, O2, and H2 on Pt. *Surf. Sci.* **1977**, *69*, 114–132.
(42) Baetzold, R. C.; Apai, G.; Shustorovich, E. The Interaction of NH3 with Ordered Pt Surfaces. *Appl. Surf. Sci.* **1984**, *19*, 134–144.
(43) Böttcher, A.; Niehus, H. Oxygen Adsorbed on Oxidized Ru(0001). *Phys. Rev. B* **1999**, *60* (20), 14396–14404. https://doi.org/10.1103/PhysRevB.60.14396.
(44) Derry, G. N.; Ross, P. N. A Work Function Change Study of Oxygen Adsorption on Pt(111) and Pt(100). *J. Chem. Phys.* **1985**, *82* (6), 2772–2778. https://doi.org/10.1063/1.448274.
(45) Madey, T. E.; Albert Engelhardt, H.; Menzel, D. Adsorption of Oxygen and Oxidation of CO on the Ruthenium (001) Surface. *Surf. Sci.* **1975**, *48* (2), 304–328. https://doi.org/10.1016/0039-6028(75)90409-4.
(46) Norton, P. R.; Goodale, J. W.; Selkirk, E. B. Adsorption of CO on Pt(111) Studied by Photemission, Thermal Desorption Spectroscopy and High Resolution Dynamic Measurements of Work Function. *Surf. Sci.* **1979**, *83*, 189–227.
(47) Onn, T. M.; Gathmann, S. R.; Wang, Y.; Patel, R.; Guo, S.; Chen, H.; Soeherman, J. K.; Christopher, P.; Rojas, G.; Mkhoyan, K. A.; Neurock, M.; Abdelrahman, O. A.; Frisbie, C. D.; Dauenhauer, P. J. Alumina Graphene Catalytic Condenser for Programmable Solid Acids. *JACS Au* **2022**, *2* (5), 1123–1133. https://doi.org/10.1021/jacsau.2c00114.
(48) Onn, T. M.; Gathmann, S. R.; Guo, S.; Solanki, S. P. S.; Walton, A.; Page, B. J.; Rojas, G.; Neurock, M.; Grabow, L. C.; Mkhoyan, K. A.; Abdelrahman, O. A.; Frisbie, C. D.; Dauenhauer, P. J. Platinum Graphene Catalytic Condenser for Millisecond Programmable Metal Surfaces. *J. Am. Chem. Soc.* **2022**, *144* (48), 22113–22127. https://doi.org/10.1021/jacs.2c09481.
(49) Oh, K.-R.; Onn, T. M.; Walton, A.; Odlyzko, M. L.; Frisbie, C. D.; Dauenhauer, P. *Fabrication of Large Area Metal-on-Carbon Catalytic Condensers for Programmable Catalysis*; preprint; Chemistry, 2023. https://doi.org/10.26434/chemrxiv-2023-bt10w.
(50) Onn, T. M.; Oh, K.-R.; Adrahtas, D. Z.; Soeherman, J. K.; Hopkins, J. A.; Frisbie, C. D.; Dauenhauer, P. J. Flexible and Extensive Platinum Ion Gel Condensers for Programmable Catalysis. *ACS Nano* **2023**, acsnano.3c09815. https://doi.org/10.1021/acsnano.3c09815.
(51) Prins, R.; Wang, A.; Li, X.; Sapountzi, F. Chapter 2. Adsorption. In *Introduction to Heterogeneous Catalysis*; World Scientific, 2022; Vol. 2.
(52) Nienhaus, H.; Bergh, H. S.; Gergen, B.; Majumdar, A.; Weinberg, W. H.; McFarland, E. W. Electron-Hole Pair Creation at Ag and Cu Surfaces by Adsorption of Atomic Hydrogen and Deuterium. *Phys. Rev. Lett.* **1999**, *82* (2), 446–449. https://doi.org/10.1103/PhysRevLett.82.446.
(53) Gergen, B.; Nienhaus, H.; Weinberg, W. H.; McFarland, E. W. Chemically Induced Electronic Excitations at Metal Surfaces. *Science* **2001**, *294* (5551), 2521–2523. https://doi.org/10.1126/science.1066134.
(54) Roldan Cuenya, B.; Nienhaus, H.; McFarland, E. W. Chemically Induced Charge Carrier Production and Transport in Pd/Si O 2/n − Si (111) Metal-Oxide-Semiconductor Schottky Diodes. *Phys. Rev. B* **2004**, *70* (11), 115322. https://doi.org/10.1103/PhysRevB.70.115322.
(55) García-Diéguez, M.; Hibbitts, D. D.; Iglesia, E. Hydrogen Chemisorption Isotherms on Platinum Particles at Catalytic Temperatures: Langmuir and Two-Dimensional Gas Models Revisited. *J. Phys. Chem. C* **2019**, *123* (13), 8447–8462. https://doi.org/10.1021/acs.jpcc.8b10877.
(56) Sze, S. M.; Ng, K. K. Chapter 1: Physics and Properties of Semiconductors-A Review. In *Physics of semiconductor devices*; Wiley-India: New Dehli, 2007; pp 7–68.

(57) Kittel, C. Chapter 6: Free Electron Fermi Gas. In *Introduction to solid state physics*; Wiley: Hoboken, NJ, 20; pp 137–141.
(58) Yang, G.; Akhade, S. A.; Chen, X.; Liu, Y.; Lee, M.; Glezakou, V.; Rousseau, R.; Lercher, J. A. The Nature of Hydrogen Adsorption on Platinum in the Aqueous Phase. *Angew. Chem. Int. Ed.* **2019**, *58* (11), 3527–3532. https://doi.org/10.1002/anie.201813958.
(59) Li, Y.; Yang, R. T. Hydrogen Storage on Platinum Nanoparticles Doped on Superactivated Carbon. *J. Phys. Chem. C* **2007**, *111* (29), 11086–11094. https://doi.org/10.1021/jp072867q.
(60) Sen, B. The Influence of Platinum Crystallite Size on H2 and CO Heats of Adsorption and CO Hydrogenation. *J. Catal.* **1991**, *130* (1), 9–20. https://doi.org/10.1016/0021-9517(91)90087-K.
(61) Dauenhauer, P. J.; Shetty, M.; Ardagh, M. A.; Pang, Y.; Abdelrahman, O. A. Electric-Field-Assisted Modulation of Surface Thermochemistry. *ACS Catal.* **2020**, *10* (21), 12867–12880. https://doi.org/10.1021/acscatal.0c02124.
(62) Graeme Henkelman, Andri Arnaldsson, Hannes Jonsson. A Fast and Robust Algorithm for Bader Decomposition of Charge Density. *Comput. Mater. Sci. 36* (3), 354–360. https://doi.org/10.1016/j.commatsci.2005.04.010.
(63) Perdew, J. P.; Burke, K.; Ernzerhof, M. Generalized Gradient Approximation Made Simple. *Phys. Rev. Lett.* **1996**, *77* (18), 3865–3868. https://doi.org/10.1103/PhysRevLett.77.3865.
(64) Langreth, D. C.; Perdew, J. P. Theory of Nonuniform Electronic Systems. I. Analysis of the Gradient Approximation and a Generalization That Works. *Phys. Rev. B* **1980**, *21* (12), 5469–5493. https://doi.org/10.1103/PhysRevB.21.5469.
(65) Kresse, G.; Joubert, D. From Ultrasoft Pseudopotentials to the Projector Augmented-Wave Method. *Phys. Rev. B* **1999**, *59* (3), 1758–1775. https://doi.org/10.1103/PhysRevB.59.1758.
(66) Kresse, G.; Furthmüller, J. Efficiency of Ab-Initio Total Energy Calculations for Metals and Semiconductors Using a Plane-Wave Basis Set. *Comput. Mater. Sci.* **1996**, *6* (1), 15–50. https://doi.org/10.1016/0927-0256(96)00008-0.
(67) Kresse, G.; Furthmüller, J. Efficient Iterative Schemes for *Ab Initio* Total-Energy Calculations Using a Plane-Wave Basis Set. *Phys. Rev. B* **1996**, *54* (16), 11169–11186. https://doi.org/10.1103/PhysRevB.54.11169.
(68) Kresse, G.; Hafner, J. *Ab Initio* Molecular Dynamics for Liquid Metals. *Phys. Rev. B* **1993**, *47* (1), 558–561. https://doi.org/10.1103/PhysRevB.47.558.
(69) Hohenberg, P.; Kohn, W. Inhomogeneous Electron Gas. *Phys. Rev.* **1964**, *136* (3B), B864–B871. https://doi.org/10.1103/PhysRev.136.B864.
(70) Kohn, W.; Sham, L. J. Self-Consistent Equations Including Exchange and Correlation Effects. *Phys. Rev.* **1965**, *140* (4A), A1133–A1138. https://doi.org/10.1103/PhysRev.140.A1133.
(71) Hjorth Larsen, A.; Jørgen Mortensen, J.; Blomqvist, J.; Castelli, I. E.; Christensen, R.; Dułak, M.; Friis, J.; Groves, M. N.; Hammer, B.; Hargus, C.; Hermes, E. D.; Jennings, P. C.; Bjerre Jensen, P.; Kermode, J.; Kitchin, J. R.; Leonhard Kolsbjerg, E.; Kubal, J.; Kaasbjerg, K.; Lysgaard, S.; Bergmann Maronsson, J.; Maxson, T.; Olsen, T.; Pastewka, L.; Peterson, A.; Rostgaard, C.; Schiøtz, J.; Schütt, O.; Strange, M.; Thygesen, K. S.; Vegge, T.; Vilhelmsen, L.; Walter, M.; Zeng, Z.; Jacobsen, K. W. The Atomic Simulation Environment—a Python Library for Working with Atoms. *J. Phys. Condens. Matter* **2017**, *29* (27), 273002. https://doi.org/10.1088/1361-648X/aa680e.
(72) Blöchl, P. E. Projector Augmented-Wave Method. *Phys. Rev. B* **1994**, *50* (24), 17953–17979. https://doi.org/10.1103/PhysRevB.50.17953.
(73) Monkhorst, H. J.; Pack, J. D. Special Points for Brillouin-Zone Integrations. *Phys. Rev. B* **1976**, *13* (12), 5188–5192. https://doi.org/10.1103/PhysRevB.13.5188.
(74) Tang, W.; Sanville, E.; Henkelman, G. A Grid-Based Bader Analysis Algorithm without Lattice Bias. *J. Phys. Condens.*

Matter **2009**, *21* (8), 084204. https://doi.org/10.1088/0953-8984/21/8/084204.

(75) Yu, M.; Trinkle, D. R. Accurate and Efficient Algorithm for Bader Charge Integration. *J. Chem. Phys.* **2011**, *134* (6), 064111. https://doi.org/10.1063/1.3553716.